JGR Oceans

RESEARCH ARTICLE
10.1029/2019JC015465

Modeling the Microwave Emission of Snow on Arctic Sea Ice for Estimating the Uncertainty of Satellite Retrievals

P. Rostosky[1], G. Spreen[1], S. Gerland[2], M. Huntemann[1], and M. Mech[3]

[1]Institute of Environmental Physics, University of Bremen, Bremen, Germany, [2]Norwegian Polar Institute, Fram Centre, Tromsø, Norway, [3]Institute for Geophysics and Meteorology, University of Cologne, Cologne, Germany

Key Points:

- The uncertainty of snow depth retrievals from satellite microwave radiometers is estimated using field measurements and model simulations
- Snow properties have the strongest contribution to the uncertainty of snow depth retrievals compared to the influence of atmosphere and ice
- The snow depth retrieval based on 19 and 7 GHz has a lower uncertainty compared to the 37 and 19 GHz one

Supporting Information:

- Supporting Information S1

Correspondence to:
P. Rostosky,
prostosky@iup.physik.uni-bremen.de

Citation:
Rostosky, P., Spreen, G., Gerland, S., Huntemann, M., & Mech, M. (2020). Modeling the microwave emission of snow on Arctic sea ice for estimating the uncertainty of satellite retrievals. *Journal of Geophysical Research: Oceans*, *125*, e2019JC015465. https://doi.org/10.1029/2019JC015465

Received 9 JUL 2019
Accepted 2 MAR 2020
Accepted article online 10 MAR 2020

©2020. The Authors.
This is an open access article under the terms of the Creative Commons Attribution-NonCommercial License, which permits use, distribution and reproduction in any medium, provided the original work is properly cited and is not used for commercial purposes.

Abstract Within a rapidly changing Arctic climate system, snow on sea ice is an important climate parameter. A common method to derive snow depth on an Arctic-wide scale is based on passive microwave satellite observations. However, the uncertainties of this method are not well constrained. In this study, we estimate the influence of geophysical parameters, including ice, snow, and atmospheric properties on passive microwave snow depth retrievals using a Monte Carlo uncertainty estimation. The results are based on model simulations from the Microwave Emission Model for Layered Snowpacks, the SNOWPACK model, and from the Passive and Active Microwave TRAnsfer model. All simulations are based on in situ observations obtained during the N-ICE2015 campaign. The average uncertainty in potential snow depth retrievals is between 11% and 19%, depending on the microwave frequencies used and increases with increasing snow depth. For lower-frequency retrievals (including 6.9 GHz), unknown snow properties are the strongest source of uncertainty while for higher-frequency retrievals (including 36.5 GHz), the contribution of ice, snow properties, and clouds is equally strong.

1. Introduction

Snow depth on Arctic sea ice is an important climate parameter. Due to its high albedo and low thermal conductivity, snow alters the radiative and energy budget of the Arctic (Webster et al., 2018), influencing the heat exchange between ocean/ice and atmosphere as well as the winter sea ice growth and summer sea ice melt (Ficheret & Morales, 1999). In addition, information about snow depth and density are needed to retrieve sea ice thickness from satellite altimetry (e.g., Kern et al., 2014; Forsström et al., 2011; Ricker et al., 2015). A strong correlation between snow depth and under-ice light fields has been found (Arndt et al., 2017), the latter being important for biological processes in the upper ocean.

Regardless of the improvements in recent coupled Arctic climate models, snow is only poorly implemented in the models (Castro-Morales et al., 2017) and important processes related to the influence of snow on the Arctic climate system are not resolved. In order to evaluate and improve snow related processes in climate models, a good, Arctic-wide snow depth product with accurate uncertainties is crucially needed (Webster et al., 2018).

Obtaining snow depth on Arctic sea ice is, however, difficult, and, so far, no routine method exists to retrieve daily snow depth over the whole sea ice covered Arctic. The most widely used methods to retrieve snow depth from space are based on passive microwave satellite observations (e.g., from AMSR-E, Comiso et al., 2003). They also provide the longest time series estimates of snow depth, by far, and are thus of special importance for climate studies. Passive microwave radiometers measure the brightness temperature (Tb) of the Earth's surface at microwave frequencies. Snow depth algorithms based on Tb measurements take advantage of the fact that snow grains scatter microwaves more when their wavelength decreases compared to the snow grain size. Scattering in the snowpack can be measured at frequencies greater than 10 GHz and becomes an important source of energy loss for frequencies around 20 GHz and higher (Mätzler et al., 2006). Since the scattering is stronger for higher frequencies (i.e., smaller wavelengths) and increases with increasing snow depth, it is possible to relate changes in the difference of two observed Tb values at different frequencies to changes in snow depth. In order to minimize the influence of the physical temperature on the observed signal, the so-called gradient ratio $GR(Tb_{v1}/Tb_{v2})$ (equation (1)) of two vertically polarized Tb values at frequency $v1$ and $v2$ is often used to estimate the snow depth using a linear relationship as described

in equation (2).

$$GR(Tb_{v1}/Tb_{v2}) = \frac{Tb_{v1} - Tb_{v2}}{Tb_{v1} + Tb_{v2}} \quad (1)$$

$$Sd = a + b * GR_{v1,v2} \quad (2)$$

In equation (2), Sd is the wanted snow depth and a and b are empirical derived regression coefficients. The first snow depth retrievals based on passive microwave satellite observations were developed for detecting snow depth and snow water equivalent on land (e.g., Chang et al., 1987). The first retrieval of snow depth on sea ice was developed by Markus and Cavalieri (1998). They derived an empirical snow depth on sea ice retrieval (similar to equation (2)), comparing the gradient ratio of passive microwave satellite observations at 18.7 and 36.5 GHz (GR(37/19)) against ship-based snow depth observations on Antarctic sea ice. However, follow-up studies (e.g., Brucker & Markus, 2013) found that the retrieval does not work over Arctic multiyear ice (MYI, ice that has survived at least one summer melt) since the scattering signal of MYI is similar to the signal of deep snow and thus makes it difficult to isolate the signal from the snow. Rostosky et al. (2018) demonstrated that, using the gradient ratio of 18.7 and 6.9 GHz (GR(19/7)), it is possible to obtain snow depth information over Arctic MYI, at least in March and April. However, Rostosky et al. (2018), and other studies examining the performance of the retrieval, concluded that the retrieval works well over level first-year ice (FYI, ice that has formed since the beginning of the freezing season) but performs poorly over deformed ice (Worby et al., 2008) and is influenced by weather effects such as warm air intrusions (Cavalieri et al., 2012). In addition, snow metamorphism can strongly influence the observed signal (Powell et al., 2006; Rostosky et al., 2018). It is clear, therefore, that further improvements in retrieval algorithms are required (Brucker & Markus, 2013; Rostosky et al., 2018). For this purpose, microwave emission models such as the Microwave Emission Model of Layered Snowpacks (MEMLS) (Wiesmann & Mätzler, 1999) or the Snow Microwave Radiative Transfer model (Picard et al., 2018) provide a useful tool. Several studies have been carried out investigating the theoretical limitations and performance of passive microwave snow depth on sea ice retrievals using microwave emission models (e.g., Markus, Cavalieri, et al., 2006; Powell et al., 2006; Willmes et al., 2014). In their modeling study Powell et al. (2006) found that GR(37/19) is strongly influenced by water vapor and clouds, while for GR(19/10) (based on 10.7 GHz instead of 6.9 GHz) only a small influence was found. Snow metamorphism was found to influence both GR(37/19) and GR(19/10). Stroeve et al. (2006) investigated on the impact of large-scale sea ice roughness on GR(37/19) and concluded that roughness has a similar effect as deep snow (i.e., over rough sea ice, GR(19/7) and GR(37/19) will be lower than over smooth sea ice Stroeve et al., 2006). Lee et al. (2018) showed that especially higher frequencies are influenced by sea ice surface roughness and that this has a strong impact on GR(37/19), especially in the transition region from FYI to MYI and over deformed ice. Using the lower frequency at 6.9 GHz (e.g., GR(19/7)), the influence of the roughness is smaller and better correlation to in situ snow depth observations can be achieved (Rostosky et al., 2018). However, the above mentioned studies mainly focus on theoretical case studies and do not provide a direct link to Arctic observations or Arctic snowpacks, which makes it is hard to constrain the limitations and uncertainties of passive microwave snow depth retrievals.

In this study, we will investigate the influence of geophysical parameters obtained from detailed field observations during the N-ICE2015 campaign (Granskog et al., 2016) on GR and derive the consequences for potential snow depth retrievals based on empirical fits similar to equation (2). The aim of this study is to estimate the uncertainties in the passive microwave snow depth products due to the influences of various geophysical parameters. The parameters investigated here are the ice properties of FYI and MYI, large-scale snow metamorphism, the atmosphere, and clouds. This paper is organized as follows. In section 2, an overview about the models and data sets used in this study is given and the experimental setups are described. In section 3, the principal results are provided. The paper follows with a discussion in section 4 and closes with a summary in section 5.

2. Data, Models, and Study Setup

The MEMLS (Wiesmann & Mätzler, 1999), adapted to sea ice (Tonboe et al., 2006), is used to simulate the surface microwave emission of snow on sea ice in dependence of ice and snow properties (see section 2.2). For estimating the influence of the Arctic atmosphere and Arctic clouds on the GR signal, the Passive and

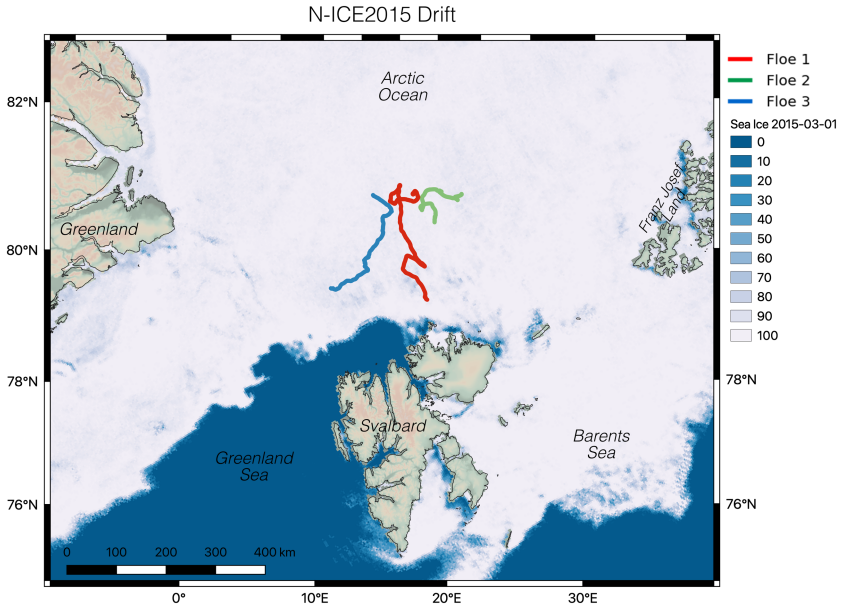

Figure 1. Map of the sea ice concentration from 1 March 2015 derived from the ASI sea ice retrieval (Spreen et al., 2008). The colored lines show the drift trajectories of the N-ICE2015 campaign for the time periods used in this study for the first floe (red; 20 January to 21 February 2015), the second floe (green; 24 February to 18 March 2015), and the third floe (blue; 19 April to 13 May 2015).

Active Microwave TRAnsfer model (PAMTRA) is used (see section 2.4). Besides snow depth, other snow properties like grain size or grain type influence the GR, the latter cannot be measured from space. In order to evaluate the complex relation between snow metamorphism and changes in the microwave emission of the snowpack, the thermodynamic snow evolution model SNOWPACK is used (Bartelt & Lehning, 2002; Lehning et al., 2002a, 2002b). All models need geophysical parameters as input data. In this study, we use snow, ice and atmospheric measurements obtained during the N-ICE2015 campaign (Cohen et al., 2017; Granskog et al., 2016; Rösel et al., 2018) as reference and input data for the models (section 2.1).

2.1. N-ICE2015 Data

The Norwegian Young ice cruise (N-ICE2015) took place from January to June 2015 north of Svalbard and in the Fram Strait, led by the Norwegian Polar Institute (Granskog et al., 2016, 2017). During the campaign, the ship was attached to four different ice floes and drifted along with them. Figure 1 shows an ice concentration map with the drift trajectories of the first three floes for time periods used in this study. In this study the focus is on the measurements from the first two floes and parts of the third floe, which cover the time period from 20 January to 18 March 2015 (floes one and two) and from 19 April to 13 May 2015 (first part of floe three). During later measurements on the third and fourth floes, the air temperature was often close to the freezing point and the snowpack became wet and slushy. Under these conditions, the relation between GR and the snow depth diminishes since wet snow is rather opaque in the microwave regime (Ulaby & Long, 2014). During the first and second floes, a winter regime with cold temperatures and moderate winds dominated. However, several storms crossed the measurement site advecting warm and moist air (Graham et al., 2017, 2019; Cohen et al., 2017). During these storms, the air temperature rose close to the freezing point and even above, which likely led to strong snow metamorphism. Figure 2 shows the time series of the 2 m air temperature and 10 m wind speed measured during the first two floes from 22 January to 18 March 2015. The storm events (e.g., 5 or 15 February) are clearly visible from the rapid increase in wind speed and high temperatures.

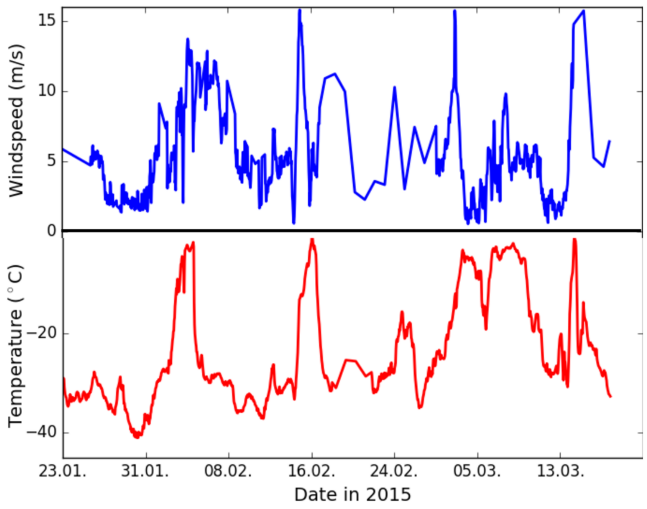

Figure 2. Two meter air temperature (bottom) and 10 m wind speed (top) measured during the first part of N-ICE2015 campaign. The data are averaged to 1 hr temporal resolution.

Table 1
Mean Snow Temperature (T), Depth (Sd), Density (ρ), and Exponential Correlation Length (e_{corr}) and Their Standard Deviation of the 28 Snow Pits Used From the N-ICE2015 Campaign Between 22 January and 13 May 2015 (Merkouriadi et al., 2017)

	Value
T (°C)	−11 ± 5
Sd (m)	0.45 ± 0.13
ρ (kg/m^3)	324 ± 43
e_{corr} (1/mm)	0.14 ± 0.03

The N-ICE2015 snow conditions are described in Merkouriadi, Gallet, Graham, et al. (2017). Snow pits were taken on FYI and second-year ice floes; however, the snow properties were similar on both floes. The snow pit measurements include snow temperature, density, grain size (maximum and minimum grain diameter), and grain type observations (based on Sommerfeld & LaChapelle, 1970). For some snow pits, specific surface area (SSA) derived from the IceCube instrument are also available. All snow measurements were taken in the vicinity of the atmospheric measurements. Overall, for the time period considered here, 28 snow pits can be used as input data for MEMLS. Table 1 shows the average snow properties of these snow pits, relevant for microwave scattering.

One important property used in MEMLS is the exponential correlation length e_{corr}. Details about the correlation length are given in section 2.2. The value of e_{corr} is related to the snow microphysics and controls the amount of microwave scattering in the snowpack; its value can be derived from SSA measurements. If SSA measurements are available, e_{corr} is calculated using equation (3) (adapted from Mätzler, 2002).

$$e_{corr} = 0.75 * \frac{4 * (1 - \phi)}{\rho_i * SSA} \tag{3}$$

In equation (3), ρ_i is the ice density and ϕ is the ratio between the measured snow density and ice density. Overall, SSA measurements were available for four snow pits. If no SSA measurements are available, it is possible to relate e_{corr} to the optical grain size (Mätzler, 2002; Grenfell & Warren, 1999). However, the grain size measured during N-ICE2015 is related to the maximum grain size (D_{max}) and can only be linked to e_{corr} for the specific case of spherical grains. Mätzler (2002) provided a lookup table for estimating e_{corr} from snow grain type, density, and D_{max} observations. This table, however, was compiled for alpine snow, and therefore, the combination of the relevant parameter obtained from the N-ICE2015 snow pits could not always be related to a specific e_{corr}.

2.2. MEMLS

The MEMLS was developed by Wiesmann and Mätzler (1999). The main objective of this model is to simulate the emissivity, transmissivity, and brightness temperature of a given snowpack for horizontal and vertical polarized microwaves. The scattering of microwaves in the snowpack is calculated using the improved Born approximation (IBA). In the IBA, the scattering in the snow is related to an exponential correlation length e_{corr} (Mätzler, 1997, 1998; Mätzler & Wiesmann, 1999). The basic idea is to treat the snow as a two-phase medium consisting of air and ice. Due to the different permittivity of air and ice, microwaves will be scattered during the propagation through the snow. The strength of the scattering depends on the wavelength and on the snow microstructure, the latter being represented by an autocorrelation function (e.g., Proksch et al., 2015; Wiesmann et al., 1998). Under the assumption that the snow is isotropic, the SSA of a snowpack can be related to the derivative of the autocorrelation function at the origin (the correlation length). The exponential correlation length, used in MEMLS, describes the length scale which is obtained by approximating the autocorrelation function by an exponential fit (Proksch et al., 2015).

$$C(\vec{r}) = C_0 * \exp\left(\frac{-|\vec{r}|}{e_{corr}}\right) \tag{4}$$

In contrast to the correlation length, the exponential correlation length (theoretically) describes the whole correlation function. In equation (4) (adapted from Proksch et al., 2015) $C(\vec{r})$ is the autocorrelation function of the lack distance $\vec{r}$, representing the snow microstructure.

The IBA was found to be an accurate approximation for scattering in snow when optical grain size is large compared to the wavelength of the microwaves (Wiesmann & Mätzler, 1999) and is valid for microwave ranges from 5 to 100 GHz (Mätzler & Wiesmann, 1999). The traditional method to estimate e_{corr} from a snowpack is an empirically derived relation between e_{corr}, the density of snow and pure ice, and the SSA (equation (3), adapted from Mätzler, 2002). MEMLS was developed for snow on land and was later adapted to sea ice (Tonboe et al., 2006). In the sea ice version of MEMLS, the model also calculates the permittivity of sea ice as a function of brine and the microwave scattering in the sea ice based on the IBA. In the version used here, a differentiation between FYI and MYI is implemented. In FYI, the scattering is controlled by

brine pockets, while air bubbles are the main scatterers for MYI, since the volume of air in MYI is much higher than the volume of brine. For both ice types, e_{corr} is, together with the inclusion volume, the most important parameter relevant for microwave scattering.

2.3. The SNOWPACK Model

The SNOWPACK model was developed to simulate the thermodynamic evolution of snow (Bartelt & Lehning, 2002). The model relates thermodynamic processes in the snow, introduced, for example, by metamorphism driven by the temperature gradient or wind-driven densification, to changes in the snow microstructure. The model is driven by external forcings and can calculate snow accumulation, melting, and metamorphism from atmospheric measurements (Lehning et al., 2002b). The model has a very detailed and complex snow microstructure scheme (Lehning et al., 2002a) using grain parameters like dentricity, sphericity, bond radius, grain size, and a so-called marker that links previous snow metamorphism to a given snowpack. These parameters, however, cannot be easily determined from field measurements. Lehning et al. (2002a) provide an overview of the relation between the above mentioned grain parameters and classical grain size and grain type observations. The dentricity of the snow grains is strongly linked to the snow age and state of metamorphism. Newly fallen snow has a dentricity close to 1 while strongly metamorphed snow with faceted snow grains or depth hoar have a dentricity close to 0. The sphericity of new snow is 0.5 and can increase or decrease depending on the environmental conditions within the snowpack (e.g., temperature gradients or snow wetness). In their paper, Lehning et al. (2002a) provide a lookup table to estimate the dentricity and sphericity of a given snowpack from traditional grain type and grain size observations. So far, no routine method exists to estimate the bond radius from traditional snow pit observations. Here we used a lookup table provided by the SNOWPACK developers (see https://models.slf.ch/p/snowpack/page/Starting-from-profiles/, accessed 15 December 2018). With the additional use of the lookup table, the N-ICE2015 snow pit measurements contain sufficient information so that the measured snow properties can be converted to the parameters relevant for SNOWPACK. Recently, SNOWPACK was adapted to sea ice (Wever et al., 2019), including sea ice relevant processes such as thermodynamic ice growth, flooding, and heat transport between the ocean/ice and snow. The model is still in the development phase. The version used here is latest SNOWPACK sea ice release (status 10 December 2018).

2.4. The PAMTRA Model

In this study the PAMTRA model (from https://github.com/igmk/pamtra, accessed: 1 November 2018) is used to simulate the radiative transfer of microwave radiation through the atmosphere. PAMTRA is a framework written in FORTRAN90 and Python for the simulation of the transfer of passive and active radiation in a plane-parallel, one-dimensional, and horizontally homogeneous cloudy atmosphere. PAMTRA makes use of the RT4 model by Evans and Stephens (1995), which applies the doubling and adding method to solve the passive radiative transfer. It is limited to the microwave frequency between 1 GHz and up to 1 THz. With PAMTRA, it is possible to simulate upwelling and downwelling radiation at any height and observation angle. The model provides radiances or polarized brightness temperatures. The PAMTRA radar simulator estimates the full radar Doppler spectrum and can derive the radar moments (e.g., skewness, kurtosis, and left and right slopes). The principles of the radar simulator are based on the concept of Kollias et al. (2011) and Kollias et al. (2014). The atmospheric input to PAMTRA can be artificial, from radiosondes or any other profiling in situ measurement. For this purpose, Python-based importers for various atmospheric models and many other data types are provided with the code.

For the calculation of the interaction parameters between radiation and atmosphere or ground, the model utilizes well-known and established methods and modules created by various authors and made publicly available. The gaseous absorption for oxygen, water vapor, and nitrogen is by default, and in this study, calculated by the Rosenkranz 98 absorption model (Rosenkranz, 2015) including recent modifications of the water vapor continuum absorption presented in Turner et al. (2009) and the line width modification of the 22.235 GHz H_2O line as proposed by Liljegred et al. (2005). An unlimited number of hydrometeor types can be described by different implemented particle size distributions. The parameters to these distributions can be adjusted so that the microphysical assumptions in the radiative transfer are consistent with the one made in the input source, that is, the atmospheric models. Single scattering and absorption properties for the hydrometeors can be calculated by various methods. These include the cost-effective Mie theory, and the more time consuming T-Matrix theory by Mischenko and Travis (1994). PAMTRA also allows the use of scattering databases that are usually created by applying the Discrete Dipole Approximation Method. For aggregates or more complex particles, PAMTRA also includes a very recent approximation called the

Table 2
Mean Snow and Sea Ice Density (ρ), Salinity (S), Exponential Correlation Length (e_{corr}), Temperature (T) at the Snow-Ice Interface and Superimposed Layer Depth (d_{SSI}), and Their Standard Deviations Used for the Sensitivity Study

	FYI	MYI	Snow top	Snow bottom
ρ (kg/m^3)	910 ± 8	800 ± 81	290	310
S	5–8 ± 0.81	0 ± 0.81 (S > 0)	0	0
e_{corr} (1/mm)	0.15 ± 0.07	0.28 ± 0.07	0.11	0.13
d_{SSI} (m)	0	0.40 ± 0.31		
T (K)	260 ± 1	260 ± 1		

Note. The sea ice properties are obtained from Fung and Eom (1982), Grenfell (2015), and Shokr and Sinha (1999).

self-similar Rayleigh-Gans Approximation (Hogan & Westbrook, 2014; Hogan et al., 2017) that is rather cost-effective compared to Discrete Dipole Approximation Method calculations. For the lower boundary, the reflectivity and emissivity properties must be provided. For the ocean, this can be done by the Tool to Estimate Sea-Surface Emissivity from Microwaves to sub-Millimeter waves (TESSEM2 Prigent et al., 2017) that is built around the community model FAST microwave Emissivity Model (FASTEM; Liu et al., 2011). For land surfaces the Tool to Estimate Land Surface Emissivity from Microwave to Submillimeter Waves (TELSEM2; Aires et al., 2011; Wang et al., 2017) has been implemented, which provides the emissivities based on geographic location and month derived from satellite measurements.

PAMTRA has been successfully used in recent years in a variety of studies considering passive and active applications (Acquistapace et al., 2017; Cadeddu et al., 2017; Ebell et al., 2013; Küchler et al., 2018; Maahn & Löhnert, 2017).

2.5. Study Setup

In order to estimate the influence of the natural variability of geophysical parameters on satellite snow depth retrievals, the following experiments were set up. The influence of the ice properties was estimated using a simplified snowpack, consisting of two layers. The snow properties of each layer are summarized in Table 2. A linear temperature profile is assumed in the snow in such a way that the temperature at the snow-ice interface is always −13 °C (this ensures that the temperature at the top of the snowpack is always negative). The ice thickness is set to 2 m and split into 2 cm thick layers. For each snow thickness, 1,000 simulations for both FYI and MYI are performed and, in every individual simulation, the ice properties are varied around a Gaussian PDF with means and standard deviations given in Table 2.

Unfortunately, only limited ice density measurements are available from the N-ICE2015 campaign. Therefore, we use reference values for the ice properties reported in several earlier studies. The reference values for the ice density are obtained from Shokr and Sinha (1999) and Fung and Eom (1982). The exponential correlation length and its standard deviation for MYI were calculated based on the air bubble diameters found by Shokr and Sinha (1999) using the same method as for the snow (Mätzler, 2002). However, this relationship is only valid under the assumption of a two-phase medium (i.e., no brine) and spherical inclusions (i.e., only air bubbles are considered). The first holds for the top layers of the MYI where superimposed ice may exist, which is almost salt free. The depth of this superimposed ice (d_{SSI}) can vary between a few centimeters up to 40 cm (i.e., Fung & Eom, 1982; Grenfell, 2015; Shokr & Sinha, 1999). Below the super imposed ice, MYI with an average density of 880 kg/cm^3 and a linear salinity profile from 1 to 4 is assumed. In addition, a linear temperature profile is assumed for both, FYI and MYI.

In their study, Shokr and Sinha (1999) found a mean circularity of 0.68 for air bubbles in MYI, which means that the air bubble inclusions in the ice are not perfectly spherical. Therefore, the assumption of spherical air bubbles introduces an error and the calculated e_{corr} might lead to an overestimation or underestimation of the actual scattering. In the case of FYI, which still contains brine pockets and a brine layer on top or in the lower snow, the penetration the penetration of the microwaves is limited to a few centimeters, and therefore, e_{corr} does not play a major role since volume scattering in FYI is generally low (see Goginen et al., 1990; Lee et al., 2018). Due to the MYI properties (lower density, almost salt free) microwaves can penetrate

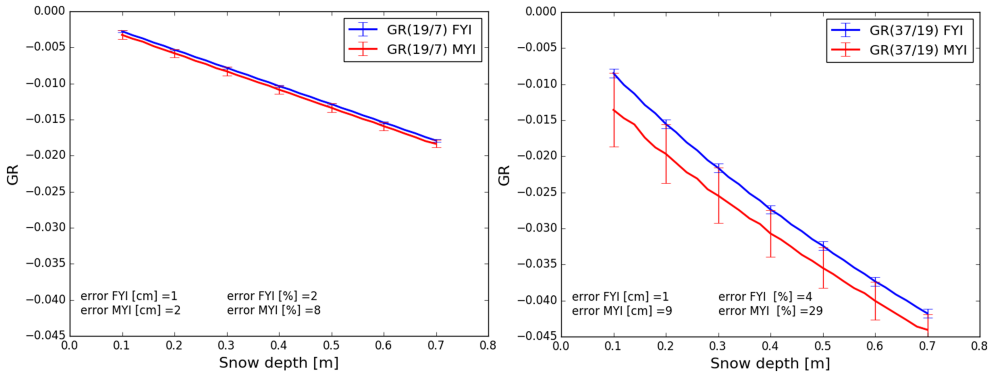

Figure 3. Sensitivity of GR(19/7) (left) and GR(37/19) (right) to FYI properties (blue) and MYI properties (red). The thick line represents the mean over the 1,000 Monte Carlo simulations and the error bar the standard deviation. In addition, the mean error of potential snow depth retrievals is shown.

up to several decimeters into the ice (Ulaby & Long, 2014). Typical air bubbles in the MYI lead to a scattering of microwaves and thus influences the GR in a similar way as deep snow.

The influence of the atmosphere on the GR is estimated using the same snowpack as described above. Then the top of the atmosphere brightness temperatures is calculated using PAMTRA and meteorological observations obtained from N-ICE2015 campaign. Overall, 258 simulations were performed based on all available radiosonde profiles obtained during the N-ICE2015 campaign. Clouds cannot be directly measured from radiosondes. However, since clouds can have a strong impact on GR, the cloud liquid water content (CLW) in the atmosphere was estimated using the modified adiabatic cloud model proposed by Karstens et al. (1994). Overall, based on this model, clouds were detected in 77 out of 258 profiles with an average CLW of 0.29 kg/m^2. Most of the clouds were low level clouds with a cloud base between 500 and 1,000 m and the cloud top was always below 5,000 m. Besides clouds, also the total column water vapor is relevant for microwaves (Ulaby & Long, 2014). The mean total column water vapor in this data set is 4.58 kg/m^2 with a standard deviation of 3.18 kg/m^2. Two studies are performed. In the first study, only the influence of atmospheric properties (excluding clouds) on the GR is investigated based on the 258 radiosonde profiles. In the second study, the influence of clouds on GR is investigated based on the 77 radiosonde profiles including the CLW profiles derived from Karstens et al. (1994). At the microwave frequencies used in this study, the absorption of radiation by water vapor is relevant, which is stronger at 37 GHz compared to 18.7 or 6.9 GHz (e.g., Smith, 1982). In addition, absorption and volume scattering by hydrometeors in clouds influences the microwave radiation observed at top of the atmosphere, both increasing with increasing frequencies (e.g., Battagia et al., 2006). The strength of the latter depends on the assumptions made about the cloud droplet properties and the cloud-scattering scheme used in PAMTRA. Here we use the model based on the Mie theory (see section 2.4) and a mixture of ice and liquid water droplets, based on results from an ECHAM5 simulation over Arctic sea ice for typical Arctic winter conditions.

3. Results

3.1. Influence of Ice Properties

For microwave observations, it is important to distinguish between Arctic FYI and MYI since both have different microwave signatures. Here, we focus on how the natural variability of the ice properties influences the GR using the study setup described in section 2.5.

Figure 3 shows the results of the Monte Carlo simulation for GR(19/7) (left) and GR(37/19) (right) for FYI (blue) and MYI (red). The thick lines represent the mean of the Monte Carlo simulations and the error bars show the standard deviation. For visualization purpose, the error bars are displayed every 10 cm. In addition, the resulting error for potential snow depth retrievals (%) is shown. This error is calculated as follows: First, a simple linear regression model is used to retrieve a theoretical snow depth Sd_n using equation (2) and the averaged GR. A second snow depth Sd_e is derived adding the standard deviation to the GR for every snow depth. The error shown in Figure 3 is the normalized root-mean-square deviation (NRMSD) between Sd_n and Sd_e. For FYI the influence of the ice properties on the GR is very small and the error is only 2% for both GR. For MYI, the influence of the ice properties on GR(19/7) remains small (standard deviation

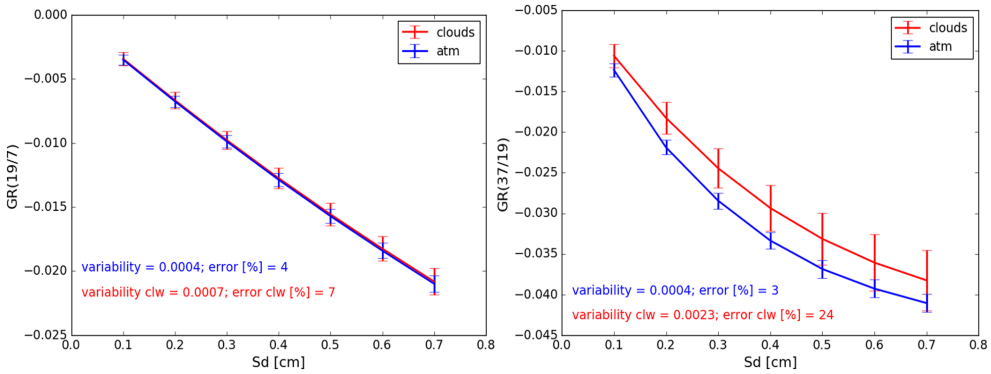

Figure 4. Sensitivity of GR(19/7) (left) and GR(37/19) (right) to atmospheric properties and clouds. The thick lines represents the mean of all 258 simulations and the error bar the variability in GR due to the cloud-free atmosphere (blue) and cloudy atmosphere (red).

is between 0.00036 and 0.00042), and, more important, is smaller than its sensitivity to snow depth (roughly 0.003/10 cm). The error due to changes in ice properties is around 8% of the actual snow depth. For GR(37/19), the influence of the MYI properties is one magnitude larger than for GR(19/7) and the potential error due to the variability of MYI properties is 29%. This is consistent with earlier findings that GR(37/19) cannot be used to retrieve snow depth for MYI, since the signal of the MYI at GR(37/19) is of similar strength than the signal of snow (e.g., Brucker & Markus, 2013; Rostosky et al., 2018).

Rostosky et al. (2018) found a reasonable correlation between GR(19/7) and snow depth on MYI, indicating that it is possible to derive a retrieval for snow depth on MYI using GR(19/7), even though the correlation between GR(19/7) and snow depth was lower for MYI than for FYI and high errors were found for MYI. Also, the results found in this study indicate that MYI properties have only little influence on GR(19/7). However, the lower correlation and increased error between GR(19/7) and snow depth on MYI found by Rostosky et al. (2018) is not visible in the modeled results shown here. This can have several reasons. The influence of large-scale roughness (e.g., from pressure ridges) on the GR is not considered here. However, this roughness has a strong impact on the GR, especially at lower frequencies (Worby et al., 2008). Second, the implementation of MYI in MEMLS is simplified regarding the calculation of volume scattering in a way that it is considered as a two-phase medium consisting of air and ice. The influence of brine on the scattering is neglected in the model, which could lead to an underestimation of the scattering in MYI.

While the focus of the other experiments are based on N-ICE2015 data sets, only a few ice core measurements over MYI were taken during the campaign. The variability of ice properties from the N-ICE2015 observations is smaller than the values found in literature. For the MYI, the mean density and variability of the ice is around 850 ± 50 kg/m^3. The salinity of the top layers vary between 0 and 2 ppt, which is similar to the values used in this study. No estimation of the air bubble size distribution for the N-ICE2015 cores was performed so far. However, using the same e_{corr} but the density variability based on MYI cores from N-ICE2015, the NRMSD between Sd_n and Sd_e is ±6% for GR(19/7) and ±24% for GR(37/19). The variability in the FYI properties is low compared to the variability of MYI properties. To test if the low NRMSD obtained for FYI is only a result of this low variability, we artificially increased the variability of the FYI properties to ±50 kg/m^3 for the density and to ±0.25 for e_{corr}. This added variability, however, still only increased the NRMSD by below 1%. Thus, we can exclude the low FYI properties variability as main error source.

3.2. Influence of the Atmosphere

As described in section 2.5, PAMTRA is used to investigate the influence of the atmosphere and clouds on the GR. Figure 4 shows the influence of the atmosphere and clouds on GR(19/7) (left) and GR(37/19) (right). The error (%) is derived in a similar way as described in section 3.1. For both GR, the influence of the atmosphere is rather low and results in a NRMSD of ±4% for a GR(19/7) based snow depth retrieval and ±3% for a GR(37/19) based snow depth retrieval. The NRMSD due to clouds is +7% at GR(19/7) and +24% at GR(37/19). Based on these results, GR(19/7) is less influenced by the atmosphere and clouds and is therefore more suited to retrieve snow depth over FYI if no atmospheric corrections are applied.

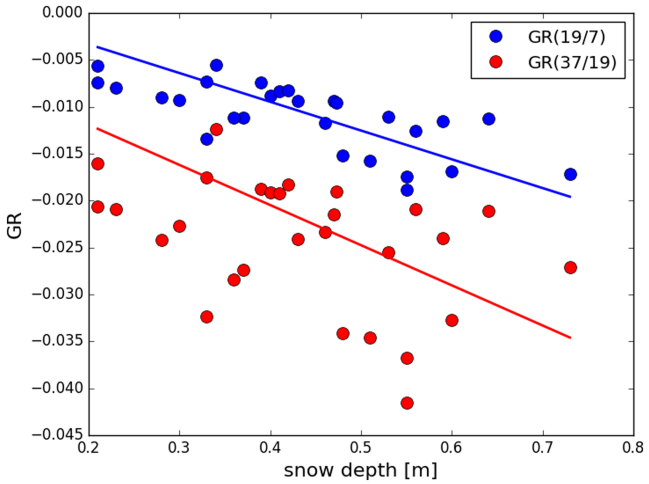

Figure 5. GR based on MEMLS simulations of the 28 snow pits used from the N-ICE2015 campaign. In addition, the regression lines are shown.

The results found here are in good agreement with the results from Markus, Powell, et al. (2006), who found a strong influence of the atmosphere and cloud liquid water on GR(37/19) but only a weak influence on GR(19/10).

3.3. Influence of Snow Properties

The snowpack properties observed during the N-ICE2015 campaign show a high variability in space and time (Merkouriadi, Gallet, Graham, et al., 2017), especially in their properties relevant for microwave scattering. Figure 5 shows GR(19/7) and GR(37/19) for all 28 snow pits calculated using MEMLS. The full initialisation files for all snowp its are provided in the supporting information. Although some relation between GR and snow depth is visible (the correlation between the GR and the snow depth is −0.7 for GR(19/7) and −0.4 for GR(37/19)), the overall scatter is very high for both GR. The RMSD between the measured snow depth and the snow depth calculated from the simulated GR and the fitting lines shown in Figure 5 are 9.7 cm for GR(19/7) and 12.5 cm for GR(37/19). However, these results probably display the effect of local variability in the snow properties and, if compared to the variability on the scale of satellite footprints, part of the variability should average out. Therefore, it is more important to consider how large-scale phenomena such as warm air inflow influence the snowpack and, consequently, the GR. Cavalieri et al. (2012) showed that warm air intrusions have a strong impact on the snow depth derived from GR(37/19) based snow depth retrievals due to the potential formation of melt/refreeze layers in the snow.

Different from previous studies, the extensive observations of ice, snow, and atmospheric properties obtained during the N-ICE2015 campaign provide the opportunity to link atmospheric measurement to snow metamorphism using a snow evolution model and to calculate its influence on the microwave signal using MEMLS. During the campaign, several storms crossed the measurement site and advected warm and moist air (Figure 2) and therefore likely introduced strong snow metamorphism. Here, we perform a case study on the snow metamorphism introduced by the storm event around the 5 February 2015 using the thermodynamic snow evolution model SNOWPACK (see section 2.3) in addition to MEMLS. For this purpose, SNOWPACK is initialized with the N-ICE2015 snow pit measurement obtained on the 23 January 2015 and then run until the 1 March 2015 using the atmospheric observations obtained during the N-ICE2015

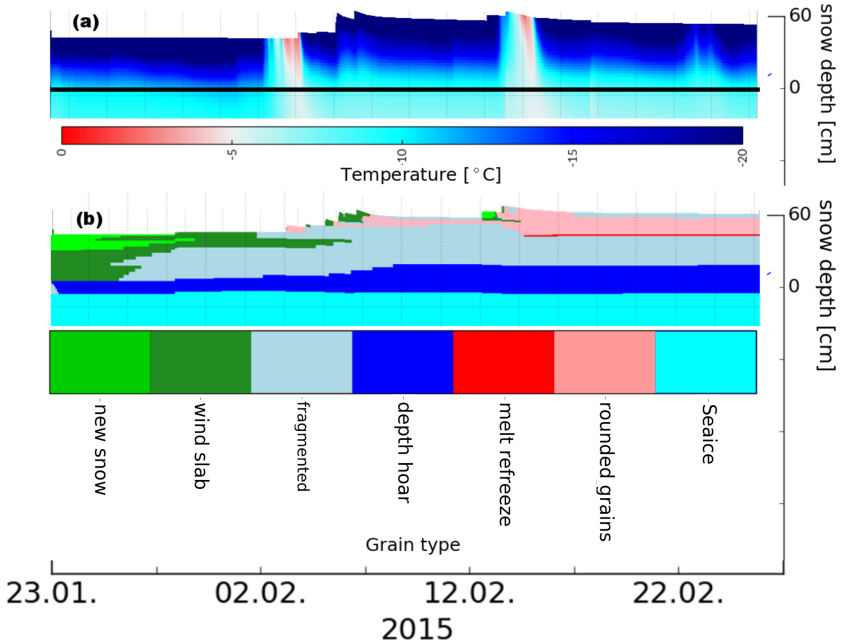

Figure 6. Time series of the snowpack temperature in °C (a) and grain type (b) based on SNOWPACK simulations from 23 January to 1 March 2015 The black line in (a) marks the snow-ice interface.

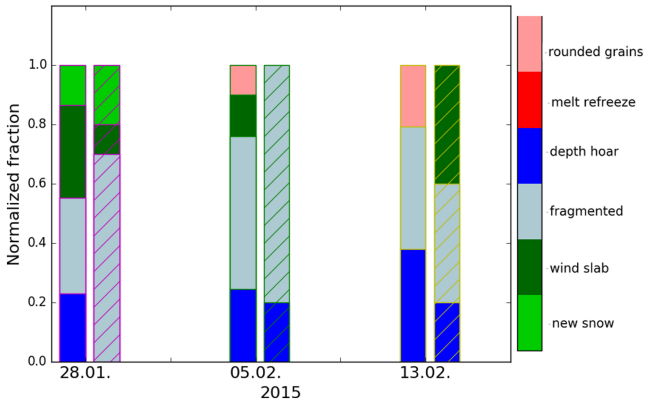

Figure 7. Comparison of three distinct grain type profiles simulated with SNOWPACK and the according N-ICE2015 measurements (hatched shaded bars). The edge colors (i.e., magenta for Snow Pit 1, green for Snow Pit 2, and yellow for Snow Pit 3) are chosen according to the colors in Figure 8.

campaign. SNOWPACK needs information about snow grain properties that were not measured in the N-ICE2015 snow pits and therefore must be estimated from the available grain related measurements and the methods described in section 2.3. The initialisation profile for the SNOWPACK simulation is provided in the supporting information.

The initial temperature profile of the simulations shows a strong negative gradient in the snow which is typical for a cold, Arctic snowpack (see Figure 6a). Around 5 February 2015, a storm advected warm air into the measurement area and the temperature gradient changes its sign, rising close to the freezing point at the snow surface. Two days after the storm, the temperature falls again and the temperature profile looks similar to the profile before the storm happened. Figure 6b shows the temporal evolution of the snow grain type. At the beginning, the top layer of the snowpack consists of newly fallen snow (13 cm) followed by a layer of wind slab (27 cm). At the bottom layer, depth hoar (11 cm) exists. From the 25 January to 2 February, the layer of new fallen snow transforms into wind slab and the wind slab layer in the middle of the snowpack transforms into fragmented snow. During the storm (5 February), a layer rounded grains forms at the top of the snowpack. In contrast to the temperature profile, the short period of warm air temperature during the storm has a long-term impact on the snow grain type.

In Figure 7, the snow type simulated by SNOWPACK is compared to snow type measurements from N-ICE2015 (modified from Merkouriadi, Gallet, Liston, et al., 2017) obtained at the 28 January (Snow Pit 1, cool conditions before the storm), at the 5 February (Snow Pit 2, during the storm), and at the 13 February (Snow Pit 3, cool conditions after the storm). Even though snow pit surveys are destructive and therefore cannot be obtained at the exactly same spot relative to the ice floe, they allow a rough comparison with the simulated snowpack to check if the overall snow evolution was modeled correctly. The grain types of Snow Pits 1 and 2 are in a good agreement with the simulated snow pits. The transformation into a snowpack with predominantly fragmented snow is visible in both data. In the third snow pit a layer of wind slab snow was found while in the model simulations, a 5 cm thick layer of rounded grains has formed at the top of the snowpack.

In order to evaluate the influence of the snow metamorphism on the GR, a MEMLS study is set up using the simulated snow profiles by SNOWPACK (see Figure 7) as input data. In order to obtain a full picture, the properties of the simulated snow profiles were scaled to 1 and then transferred to a snowpack varying from 2 to 70 cm with 2 cm steps. Figure 8 shows the results of the MEMLS simulation using the above mentioned snow profiles as input for GR(19/7) (left) and GR(37/19) (right). Two additional, artificial snow profiles were added in order to cover a wider range of possible snowpacks. These profiles are similar to Profile 1 in Figure 7 but contain a fraction of 20% new fallen snow at the top (red curve) or 20% slightly compacted snow (blue curve). These types of snow profiles were not observed during N-ICE2015 campaign because

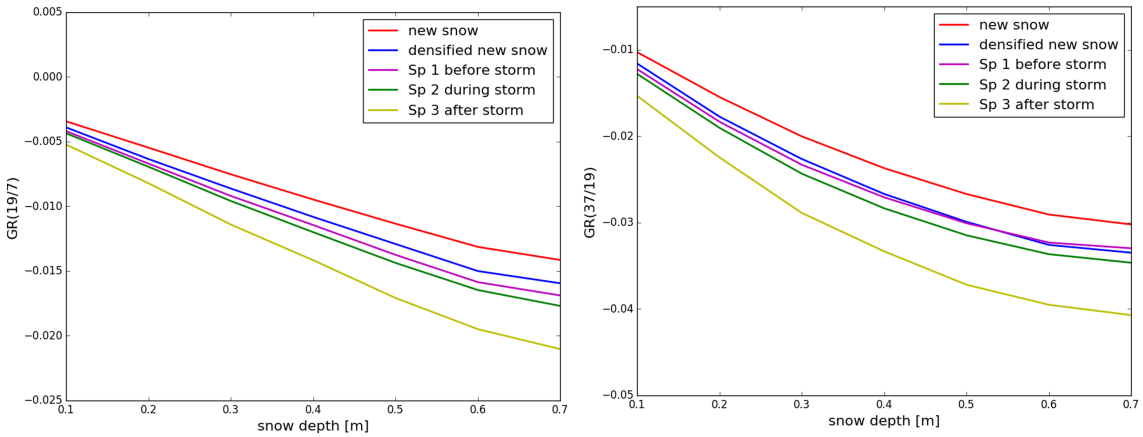

Figure 8. GR(19/7) (left) and GR(37/19) (right) for five snowpack with different snow properties.

Table 3
Standard Deviation of GR Due to the Variability in Atmospheric and Snow Properties As Well As Clouds

	GR(19/7)	GR(37/19)
Atmosphere	±0.0004	±0.0005
Clouds	0.0007	0.0023
Snow	±0.0013	±0.0026

it only started in January after the initial snow fall events in fall. The N-ICE2015 snowpack is representative for spring snow conditions, where the snow is compacted and has undergone metamorphism. During the Surface Heat Budget of the Arctic Ocean campaign, which took place from October 1997 to October 1998, the most predominant snow types observed consisted of predominantly depth hoar, wind slab, and fresh snow (Sturm et al., 2002). With the addition of the two above mentioned snowpacks, the simulations cover also early winter snow conditions. From Figure 8 we see that both, GR(19/7) and GR(37/19) strongly depend on the snow type. Especially the snow pit that was simulated after the storm event (yellow curve) leads to significant lower GR than the snow pits before and during the storm. With the addition of the "new fallen" snow, these simulations should cover a good amount of variability which can be expected over large scales in the whole Arctic. Overall, the NRMSD, calculated as described in section 3.1, is similar for both GRs and is around 20% for GR(19/7) and 24% for GR(37/19).

3.4. Uncertainty of Snow Depth Retrievals

From the uncertainties in GR derived in this study, it is possible to estimate the uncertainty of GR-based snow depth retrievals due to unknown state of the atmosphere and unknown snow type. To investigate this, the following study is set up: Based on the individual results from each study (see sections 3.1–3.3), a set of 2,580 simulations are available, each simulation with slightly different conditions for the atmosphere, clouds, and snow type. From these simulations the standard deviation of the GR due to each quantity can be obtained (see Table 3). Then, a 1,000-member Monte Carlo simulation is performed for a snowpack varying between 2 and 70 cm. In each simulation and for each snow depth, a random error between ± the standard deviation from the three types of uncertainty sources (snow type, atmosphere, and clouds) is added to the averaged GR(19/7) and GR(37/19) (in the following called GR_{noise}). Then, a linear regression is performed between GR_{noise} and the snow depth and the regression coefficients are used to retrieve a snow depth. This retrieved snow depth is then compared to the real snow depth. With this method, it is possible to estimate the uncertainty of a snow depth retrieval if no information about the snow type, the state of the atmosphere or clouds are available during the training of the retrieval under the assumption that all quantities vary in the training data set.

The first two columns in Table 4 are the results of the reference regression analysis based on an GR without any uncertainties are shown (in the following called GR_{mean}). Here the NRMSD is related to the normalized RMSD introduced for assuming a linear model. For GR(19/7), the assumption of an linear relation between GR and the snow depth leads only to small errors (NRMSD ≤ 2%). However, for a retrieval based on GR(37/19), the linear assumption results in an NRMSD of 10% for the snowpack investigated here. This is mainly due to the nonlinear relation between GR(37/19) and snow depths >50 cm (as can be seen in Figure 8, right). We performed the same analysis limiting the snow depth to 50 cm and found an NRMSD for GR(37/19) based retrievals of 4%. The results of the Monte Carlo simulations including the uncertainties of GR derived in section 3 (see Table 3) are shown in the third and fourth columns of Table 4. Here, the mean regression coefficients over all 1,000 simulations are shown together with their standard deviation, along with the NRMSD and correlation between the snow depth retrieved from GR_{noise} and the input snow depth. The NRMSD increases in both models to 11% for the GR(19/7) and to 19% for the GR(37/19) based retrieval. These results demonstrate the need for additional data in GR-based snow depth retrievals, since otherwise the retrieval has mean error of at least 11%. The influence of, for example, sea ice roughness on the GR is

Table 4
Regression Coefficients and Error Statistics of GR-Based Snow Depth Retrievals Without ($GR(v1,v2)_{mean}$; Columns 1 and 2) and With Uncertainties ($GR(v1,v2)_{noise}$; Columns 3 and 4) in the GR

	$GR(19/7)_{mean}$	$GR(37/19)_{mean}$	$GR(19/7)_{noise}$	$GR(37/19)_{noise}$
Slope	−3,900	−2,300	−3,000 ± 230	−1,500 ± 140
Intercept	−0.04	−0.19	0.06 ± 0.03	0.02 ± 0.04
Correlation	−0.99	−0.98	−0.99	−0.98
NRMSD (%)	2	10	11	19

not considered in this study. In addition, the training of satellite retrievals will always contain errors due to resolution differences between the satellite observations and the snow depth measurements. Therefore, the real error of GR-based snow depth retrievals could be higher than the errors found here. On the other hand, the employed models might contain uncertainties, which are not present in the observations.

The variability in the regression coefficients gives an indication about the robustness of the fit. For both retrievals, the standard deviation of the regression coefficients is less than 10% for the slope and 3 to 4 cm for the intercept (Columns 3 and 4 in Table 4).

The strongest contribution to the NRMSD of the retrieved snow depth is due to the uncertainties obtained from the different snow types. Assuming the snow type is known (e.g., zero uncertainty for the snow type), the NRMSD of the GR(19/7)-based retrieval would decrease to 4%, which is close to ideal case (i.e., no uncertainties in GR) and for GR(37/19) to 13%. Adding information about the atmosphere leads to an improvement on the results of GR(37/19) reducing the NRMSD to 15%. In addition, the variability in the regression coefficients reduces with a reduced uncertainty in GR.

4. Discussion

The findings in section 3.4 have consequences for retrievals of snow depth on Arctic sea ice based on the GR values. The results demonstrate that if a GR-based snow depth retrieval is trained without adding information about properties influencing the GR, high potential errors in the derived regression coefficients can be the result. However, even if information about snow type and the clouds are available during the training, they also need to be considered during daily retrieval in order to improve the snow depth retrievals (e.g., Cavalieri et al., 2012). Notably, a good knowledge of the snow type is crucial for improving GR-based snow depth retrievals. For snow on land, studies have shown that it is possible to link snow metamorphism relevant for microwave scattering to the vertical temperature gradient in the snow (e.g., Josberger & Mognard, 2002). Other attempts assimilate observations from measurement data into a thermodynamic snow evolution model for improving satellite-derived snow depth retrievals (e.g., Pulliainen, 2006). On sea ice, however, weather observations from stations are rare. Ice mass balance buoys drifting on the ice can provide snow depth and temperature profiles, which, however, are valid only for a small scale around the buoy. For snow on sea ice, the thermodynamic modeling of snow evolution is still part of ongoing work and faces difficulties. Simple relations between the air temperature and the snow metamorphism as derived for snow on land might not be possible due to the sea ice drift and unknown heat fluxes through the ice causing snow metamorphism at the bottom. If information about the initial snow profile and ice properties are known, thermodynamic snow models (e.g., SNOWPACK) are able to simulate the influence of large-scale effects like warm air intrusions on snow evolution as shown in this study. Models constrained by observations could, therefore, provide a way forward for improved satellite retrievals.

The results shown here are all based on models and thus subject of assumptions and simplifications. This is particularly important for the results shown in Figures 5 and 8. In order to simulate these brightness temperatures, the scattering parameter e_{corr} had to be estimated from a lookup table (Mätzler, 2002). In addition, thin ice crusts were present in most of the snow pits observed during the N-ICE2015 campaign. However, these ice crusts are not resolved in MEMLS. Therefore, the variability of the GR in dependence of the snow type might be too low and the derived uncertainty for GR-based snow depth retrievals underestimated. In the simulations for Figure 8, the different layers within the snowpack were equally scaled from 2 to 70 cm. While this may not be the most realistic approach, not enough information about the evolution of the Arctic snowpack is available to derive a more sophisticated approach.

5. Conclusions

In this study, the influences of the atmosphere, clouds, snow, and ice properties on the GR are estimated based on model simulations using the MEMLS, the passive and active radiative transfer model PAMTRA and the thermodynamic snow model SNOWPACK. All results are based on in situ ice, snow, and atmospheric measurements obtained during the first part of the N-ICE2015 campaign (winter conditions). We found that the (cloud free) atmosphere has only little influence on both, GR(19/7) and GR(37/19). For GR(19/7), the biggest source of uncertainty is the variability in the snow properties. Based on a case study for snow metamorphism introduced by warm air advection, we find an uncertainty in the GR(19/7) of about 20% due to different snow types. For GR(37/19) the influence of clouds and snow metamorphism are of similar range

and are 24% for snow metamorphism and 29% for clouds. The ice properties have only a strong influence on GR in the case of Arctic MYI. Here, the uncertainty is around 8% for GR(19/7) and 29% for GR(37/19). However, the results for the influence of the MYI properties on the GR are lower than what is found in satellite observations. This potentially is due to the simplifications made in the model used here. The influence of the ice roughness on the GR is not investigated.

With the uncertainties in GR derived here, it was evaluated how these uncertainties influence the performance of potential GR-based snow depth retrievals. In the ideal case, without any uncertainties in GR, the GR(19/7) based retrieval performs best. The NRMSD of a GR(19/7)-based retrieval is around 2% and for GR(37/19) 10%. Including the uncertainty of the GR to the regression analysis using a Monte Carlo simulation (only for FYI), all NRMSD increase. The NRMSD of GR(37/19) increases to 19%, of GR(19/7) to 11%. These modeling results show that it is possible to derive snow depth from GR of microwave brightness temperatures despite large variability in the snow, ice, and atmosphere geophysical parameters. Overall, the GR(19/7) performs best, which is also confirmed by satellite observations (Rostosky et al., 2018). However, if no information about the geophysical state of the snow and atmosphere is used there are significant uncertainties for the derived snow depth. Thus, these results show the importance of adding additional information to GR-based passive microwave-based snow depth retrievals during both the training and operational use. While an estimation of the influence of the atmosphere and clouds on the brightness temperatures observed by satellite is already applied in for, example, passive microwave sea ice concentration retrievals (e.g., Lu et al., 2018), adding information about the snow type remains difficult since measurements are sparse and thermodynamic snow evolution modeling is challenging. In the upcoming MOSAiC campaign, an extensive data set of year round snow and ice properties will be collected. The data that will be collected during MOSAiC might help to improve the understanding of snow processes relevant for microwave scattering and help to reduce uncertainties in passive microwave-based snow depth on Arctic sea ice retrievals.

The variability in GR due to the influence of geophysical parameters found in this study are not limited to passive microwave snow depth retrievals. They can also, after a few adjustments, be used to evaluate the sensitivity of other related sea ice parameter retrievals that are using similar microwave frequencies. These are, for example, sea ice concentration retrievals like the NASA-Team (Markus & Cavalieri, 2000) or the ASI algorithm (Spreen et al., 2008).

Appendix A: N-ICE2015 Snow Pit Data

The snow pit data used in this study can be downloaded from the Norwegian Polar Data Centre (doi: 10.21334/npolar.2017.d2be5f05, accessed 2 November 2017). In Table A1, all selected snow pits used in this study are listed. In addition, the air temperature (T) during the measurement of the snow pit is given.

Table A1
Date, Latitude, Longitude, and Number of the N-ICE2015 Snow Pit Data Used for This Study

Date in 2015	Latitude (°N)	Longitude (°E)	Number	T (°C)
20 January	83.15	20.07	1	−21.8
23 January	83.10	20.67	2	−33
23 January	83.10	20.68	3	−32.9
28 January	83.07	17.95	4	−28.8
28 January	83.06	19.95	5	−26.9
28 January	83.06	17.95	6	−28.3
3 February	83.08	16.48	7	−9
3 February	83.09	16.53	8	−10.7
13 February	81.95	19.70	10	−30.2
27 February	82.92	26.55	1	−34.2
2 March	82.97	25.90	2	−21.5
5 March	83.13	24.15	3	−6.7

Table A1 *(continued)*

Date in 2015	Latitude (°N)	Longitude (°E)	Number	T (°C)
7 March	83.15	23.85	4	−3.6
8 March	83.19	23.23	5	−2.8
9 March	83.17	22.06	6	−2.9
9 March	83.17	22.06	7	−3.3
10 March	83.11	21.69	8	N/A
11 March	83.02	21.32	9	N/A
13 March	82.88	21.28	10	N/A
13 March	82.86	21.23	11	N/A
18 March	82.61	22.78	12	N/A
19 April	83.11	14.25	1	−14.5
27 April	82.25	14.47	3	−11.8
27 April	82.24	14.40	4	−12.75
13 May	81.38	9.09	14	N/A
13 May	81.37	9.06	15	N/A
31 May	80.69	6.40	32	N/A
31 May	80.69	6.93	33	N/A

Note. In addition, the air temperature during the snow pit measurements is given.

Acknowledgments
We gratefully acknowledge the funding by the Deutsche Forschungsgemeinschaft (DFG, German Research Foundation)—Project 268020496—TRR 172, within the Trans-regional Collaborative Research Center "ArctiC Amplification: Climate Relevant Atmospheric and SurfaCe Processes, and Feedback Mechanisms $(AC)^3$." We would like to thank all members of the N-ICE2015 team and the crew from R/V Lance for their help collecting and producing the N-ICE2015 data set. Last, but not least, we thank Polona Itkin, Anja Rösel, and Ioanna Merkouriadi for providing the snow pit data and for their helpful comments. We thank the reviewers for their helpful comments. The data from the N-ICE2015 campaign used in this study are freely available at the Norwegian Polar Data Centre (snow pit data: https://doi.org/10.21334/npolar.2017.d2be5f05, accessed 2 November 2017; atmospheric data: https://doi.org/10.21334/npolar.2015.056a61d1, accessed 10 June 2018).

References

Acquistapace, C., Kneifel, S., Löhnert, U., Kollias, P., Maahn, M., & Bauer-Pfundstein, M. (2017). Optimizing observations of drizzle onset with millimeter-wavelength radars. *Atmospheric Measurement Techniques*, *10*(5), 1783–1802.

Aires, F., Prigent, C., Bernardo, F., Jiménez, C., Saunders, R., & Brunel, P. (2011). A Tool to Estimate Land-Surface Emissivities at Microwave Frequencies (TELSEM) for use in numerical weather prediction. *Quarterly Journal of the Royal Meteorological Society*, *137*(656), 690–699.

Arndt, S., Meiners, K. M., Ricker, R., Krumpen, T., Katlein, C., & Nicolaus, M. (2017). Influence of snow depth and surface flooding on light transmission through Antarctic pack ice. *Journal of Geophysical Research: Oceans*, *122*, 2108–2119. https://doi.org/10.1002/2016JC012325

Bartelt, P., & Lehning, M. (2002). A physical SNOWPACK model for the swiss avalanche warning. Part I: Numerical model. *Cold Regions Science and Technology*, *35*, 123–145.

Battagia, A., Simmer, C., Crewell, S., Czekala, H., Emde, C., Marzano, F., et al. (2006). Emission and scattering by clouds and precipitation. In Mätzler, C. (Ed.), *Thermal microwave radiation: Applications for remote sensing* (Vol. 52, pp. 102–117). London, UK: IEE Electromagnetic Waves Series.

Brucker, L., & Markus, T. (2013). Arctic-scale assessment of satellite passive microwave-derived snow depth on sea ice using operation icebridge airborne data. *Journal of Geophysical Research: Oceans*, *118*, 2892–2905. https://doi.org/10.1002/jgrc.20228

Cadeddu, M. P., Marchand, R., Orlandi, E., Turner, D. D., & Mech, M. (2017). Microwave passive ground-based retrievals of cloud and rain liquid water path in drizzling clouds: Challenges and possibilities. *IEEE Transactions on Geoscience and Remote Sensing*, *55*(11), 6468–6481.

Castro-Morales, K., Ricker, R., & Gerdes, R. (2017). Regional distribution and variability of model-simulated arctic snow on sea ice. *Polar Science*, *13*, 33–49.

Cavalieri, D., Markus, T., Ivanoff, A., Miller, J. A., Brucker, L., Sturm, M., et al. (2012). A comparison of snow depth on sea ice retrievals using airborne altimeters and an AMSR-E simulator. *IEEE Transactions on Geoscience and Remote Sensing*, *50*(8), 3027–3040.

Chang, A. T. C., Foster, J. L., & Hall, D. K. (1987). NIMBUS- 7 SMMR derived global snow cover parameters. *Annals of Glaciology*, *9*, 39–44.

Cohen, L., Hudson, S. R., Walden, V. P., Graham, R. M., & Granskog, M. A. (2017). Meteorological conditions in a thinner arctic sea ice regime from winter to summer during the Norwegian Young Sea Ice expedition (N-ICE2015). *Journal of Geophysical Research: Atmosphere*, *122*, 7235–7259. https://doi.org/10.1002/2016JD026034

Comiso, J. C., Cavalieri, D., & Markus, T. (2003). Sea ice concentration, ice temperature, and snow depth using AMSR-E data. *IEEE Transaction on Geoscience and Remote Sensing*, *41*(2), 243–252.

Ebell, K., Orlandi, E., Hünerbein, A., Löhnert, U., & Crewell, S. (2013). Combining ground-based with satellite-based measurements in the atmospheric state retrieval: Assessment of the information content. *Journal of Geophysical Research: Atmospheres*, *118*, 6940–6956. https://doi.org/10.1002/jgrd.50548

Evans, K. F., & Stephens, G. L. (1995). Microwave radiative transfer through clouds composed of realistically shaped ice crystals. Part II. Remote sensing of ice clouds. *Journal of Atmospheric Science*, *52*(11), 2058–2072.

Ficheret, T., & Morales, M. A. (1999). Modeling the influence of snow accumulation and snow-ice formation on the seasonal cycle of the Antarctic sea-ice cover. *Climate Dynamics*, *15*, 251–268.

Forsström, S., Gerland, S., & Pedersen, C. A. (2011). Thickness and density of snow-covered sea ice and hydrostatic equilibrium assumption from in situ measurements in Fram Strait, the Barents Sea and the Svalbard coast. *Annals of Glaciology*, *52*(57), 261–270.

Fung, A. K., & Eom, H. J. (1982). Application of a combined rough surface and volume scattering theory to sea ice and snow backscatter. *IEEE Tansaction on Geoscience and Remote Sensing*, *GE-20*(4), 528–536.

Goginen, S., Moore, R. K., Wang, Q., Gow, A., & Onstott, R. G. (1990). Radar backscatter measurements over saline ice. *International Journal of Remote Sensing*, *11*(4), 603–615.

Graham, R. M., Cohen, L., Petty, A. A., Boisvert, L. N., Rinke, A., Hudson, S. R., et al. (2017). Increasing frequency and duration of Arctic winter warming events. *Geophysical Research Letters*, *44*, 6974–6983. https://doi.org/10.1002/2017GL073395

Graham, R. M., Itkin, P., Meyer, A., Sundfjord, A., Spreen, G., Smedsrud, L. H., et al. (2019). Winter storms accelerate the demise of sea ice in the Atlantic sector of the Arctic Ocean. *Nature Scientific Reports*, *9*, 1–16.

Granskog, M. A., Assmy, P., Gerland, S., Spreen, G., Steen, H., & Smedsrud, L. H. (2016). Arctic research on thin ice—Consequences of arctic sea ice loss. *Eos, Transaction American Geophysical Union*, *97*(5), 22–26.

Granskog, M. A., Ilker, F., Rinke, A., & Steen, H. (2017). Atmosphere-ice-ocean-ecosystem processes in a thinner Arctic sea ice regime: The Norwegian Young Sea ICE (N-ICE2015) Expedition. *Journal of Geophysical Research: Ocean*, *123*, 1586–1176. https://doi.org/10.1002/2017JC013328

Grenfell, T. C. (2015). Surface-based passive microwave studies of multiyear sea ice. *Journal of Geophysical Research: Earth Surface*, *120*, 346–362. https://doi.org/10.1029/91JC02651

Grenfell, T. C., & Warren, S. G. (1999). Representation of a nonspherical ice particle by a collection of independent spheres for scattering and absorption of radiation. *Journal of Geophysical Research*, *104*(D24), 31,697–31,709. https://doi.org/10.1029/1999JD900496

Hogan, R. J., Honeyager, R., Tyynelä, J., & Kneifel, S. (2017). Calculating the millimetre-wave scattering phase function of snowflakes using the self-similar rayleigh-gans approximation. *Quarterly Journal of the Royal Meteorological Society*, *143*(703), 834–844.

Hogan, R. J., & Westbrook, C. D. (2014). Equation for the microwave backscatter cross section of aggregate snowflakes using the self-similar Rayleigh-Gans approximation. *Journal of the Atmospheric Sciences*, *71*(9), 3292–3301.

Josberger, E. G., & Mognard, N. M. (2002). A passive microwave snow depth algorithm with a proxy for snow metamorphism. *Hydrological Processes*, *16*, 1557–1568.

Karstens, U., Simmer, C., & Ruprecht, E. (1994). Remote sensing of cloud liquid water. *Meteorology and Atmospheric Physics*, *54*, 157–171.

Kern, S., Khvorostovsky, K., Skourup, H., Rinne, E., Parsakhoo, Z. S., Djepa, V., et al. (2014). The impact of snow depth, snow density and ice density on sea ice thickness retrieval from satellite radar altimetry: Results from the ESA-CCI sea ice ECV project round robin exercise. *The Cryosphere*, *9*, 37–52.

Kollias, P., Remillard, J., Luke, E., & Szyrmer, W. (2011). Cloud radar doppler spectra in drizzling stratiform clouds: 1. Forward modeling and remote sensing applications. *Journal of Geophysical Research*, *116*, D13201. https://doi.org/10.1029/2010JD015237

Kollias, P., Tanelli, S., Battaglia, A., & Tatarevic, A. (2014). Evaluation of EarthCARE cloud profiling radar doppler velocity measurements in particle sedimentation regimes. *Journal of Atmospheric and Oceanic Technology*, *31*, 366–386.

Küchler, N., Kneifel, S., Kollias, P., & Löhnert, U. (2018). Revisiting liquid water content retrievals in warm stratified clouds: The modified Frisch. *Geophysical Research Letters*, *45*, 9323–9330. https://doi.org/10.1029/2018GL079845

Lee, S.-M., Sohn, B.-J., & Shi, H. (2018). Impact of ice surface and volume scatterings on the microwave sea ice apparent emissivity. *Journal of Geophysical Research: Atmospheres*, *123*, 9220–9237. https://doi.org/10.1029/2018JD028688

Lehning, M., Bartelt, P., Brown, B., & Fierz, C. (2002b). A physical SNOWPACK model for the swiss avalanche warning part III: Meteorological forcing, thin layer formation and evaluation. *Cold Regions Science and Technology*, *35*, 169–184.

Lehning, M., Bartelt, P., Brown, B., Fierz, C., & Satyawali, P. (2002a). A physical SNOWPACK model for the swiss avalanche warning. Part II: Snow microstructure. *Cold Regions Science and Technology*, *35*, 147–167.

Liljegred, J. C., Boukabaram, S. A., Cady-Pereira, K., & Clough, S. A. (2005). The effect of the half-width of the 22-GHz water vapor line on retrievals of temperature and water vapor profiles with a 12-channel microwave radiometer. *IEEE Transactions on Geoscience and Remote Sensing*, *43*, 1102–1108.

Liu, Q., Weng, F., & English, S. J. (2011). An improved fast microwave water emissivity model. *IEEE Transactions on Geoscience and Remote Sensing*, *49*(4), 1238–1250.

Lu, J., Heygster, G., & Spreen, G. (2018). Atmospheric correction of sea ice concentration retrieval for 89 GHz AMSR-E observations. *IEEE Journal of Selected Topics in Applied Earth Observation and Remote Sensing*, *11*(5), 1442–1457.

Mätzler, C., Rosenkranz, P. W., Battaglia, A., & Wigneron, J. P. (2006). *Thermal microwave radiation: Applications for remote sensing* (Vol. 52). London, UK: IEE Electromagnetic Waves Series.

Maahn, M., & Löhnert, U. (2017). Potential of higher-order moments and slopes of the radar doppler spectrum for retrieving microphysical and kinematic properties of arctic ice clouds. *Journal of Applied Meteorology and Climatology*, *56*(2), 263–282.

Markus, T., & Cavalieri, D. (1998). Snow depth distribution over sea ice in the Southern Ocean from satellite passive microwave data. *Antarctic Research Series*, *74*, 19–39.

Markus, T., & Cavalieri, D. (2000). An enhancement of the NASA team sea ice algorithm. *IEEE Transactions on Geoscience and Remote Sensing*, *38*(3), 1387–1398.

Markus, T., Cavalieri, D., Gasiewski, A., Klein, M., Maslanik, J., Powell, D. C., et al. (2006). Microwave signatures of snow on sea ice: Observations. *IEEE Transactions on Geoscience and Remote Sensing*, *44*(11), 3081–3090.

Markus, T., Powell, D. C., & Wang, J. R. (2006). Sensitivity of passive microwave snow depth retrievals to weather effects and snow evolution. *IEEE Transactions on Geoscience and Remote Sensing*, *44*(11), 3091–3102.

Mätzler, C. (1997). Autocorrelation functions of granular media with free arrangement of spheres, spherical shells or ellipsoids. *Journal of Applied Physics*, *81*(3), 1509–1517.

Mätzler, C. (1998). Improved Born approximation for scattering of radiation in a granular medium. *Journal of Applied Physics*, *83*, 6111–6117.

Mätzler, C. (2002). Relation between grain-size and correlation length of snow. *Journal of Glaciology*, *48*(162), 461–466.

Mätzler, C., & Wiesmann, A. (1999). Extension of the microwave emission model of layered snowpacks to coarse-grained snow. *Remote Sensing of Environment*, *70*(3), 317–325.

Merkouriadi, I., Gallet, J.-C., Graham, R. M., Liston, G., Polashenski, C., Rösel, A., & Gerland, S. (2017). Winter snow conditions on arctic sea ice north of Svalbard during the Norwegian Young Sea ICE (N-ICE2015) expedition. *Journal of Geophysical Research: Atmosphere*, *122*, 10,837–10,854. https://doi.org/10.1002/2017JD026753

Merkouriadi, I., Gallet, J.-C., Liston, G., Polashenski, C., Itkin, P., King, J., et al. (2017). N-ICE2015 snow pit data. Norwegian Polar Institute. https://doi.org/10.21334/npolar.2017.d2be5f05

Mischenko, M. I., & Travis, L. D. (1994). T-matrix computations of light scattering by large spheroidal particles. *Optics Communications*, *109*, 16–21.

Picard, G., Sandell, M., & Löwe, H. (2018). SMRT: An active/passive microwave radiative transfer model for snow with multiple microstructure and scattering formulations (v1.0). *Geoscientific Model Development Discussion*, *11*(7), 2763–2788.

Powell, D. C., Markus, T., Cavalieri, D., Gasiewski, A., Klein, M., Maslanik, J., et al. (2006). Microwave signatures of snow on sea ice: Modeling. *IEEE Transactions on Geoscience and Remote Sensing*, *44*(11), 3091–3102.

Prigent, C., Aires, F., Wang, D., Fox, S., & Harlow, C. (2017). Sea-surface emissivity parametrization from microwaves to millimetre waves. *Quarterly Journal of the Royal Meteorological Society*, *143*(702), 596–605.

Proksch, M., Löwe, H., & Schneebeli, M. (2015). Density, specific surface area, and correlation length of snow measured by high-resolution penetrometry. *Journal of Geophysical Recearch: Earth Surface*, *120*, 346–362. https://doi.org/10.1002/2014JF003266

Pulliainen, J. (2006). Mapping of snow water equivalent and snow depth in boreal and sub-Arctic zones by assimilating space-borne microwave radiometer data and ground-based observations. *Remote Sensing of Environment*, *101*, 257–269.

Ricker, R., Hendricks, S., Perovich, D., Helm, V., & Gerdes, R. (2015). Impact of snow accumulation on Cryosat-2 range retrievals over Arctic sea ice: An observational approach with buoy data. *Geophysical Research Letters*, *42*, 4447–4455. https://doi.org/10.1002/2015GL064081

Rösel, A., Itkin, P., King, J., Divine, D., Wang, C., Granskog, M. A., et al. (2018). Thin sea ice, thick snow, and widespread negative freeboard observed during N-ICE2015 north of Svalbard. *Journal of Geophysical Research: Oceans*, *123*, 1156–1176. https://doi.org/10.1002/2017JC012865

Rosenkranz, P. W. (2015). A model for the complex dielectric constant of supercooled liquid water at microwave frequencies. *IEEE Transactions on Geoscience and Remote Sensing*, *53*(3), 1387–1393.

Rostosky, P., Spreen, G., Farrell, S. L., Heygster, G., Frost, T., & Melsheimer, C. (2018). Snow depth on Arctic sea ice retrieval from passive microwave radiometers—Improvements and extension to lower frequencies. *Journal of Geophysical Research: Oceans*, *123*, 7120–7138. https://doi.org/10.1029/2018JC014028

Shokr, M. E., & Sinha, N. K. (1999). Arctic sea ice microstructure observations relevant to microwave scattering. *Arctic*, *47*(3), 265–279.

Smith, E. K. (1982). Centimeter and millimeter wave attenuation and brightness temperature due to atmospheric oxygen and water vapour. In Ualby, F. T., Moore, R. K., & Fung, A. K. (Eds.), *Microwave remote sensing: From theory to applications, Volume III* (pp. 1303–1308). Annn Arbor, Michigan: University of Michigan Press.

Sommerfeld, R. A., & LaChapelle, E. (1970). The classification of snow metamorphism. *Journal of Glaciology*, *9*(55), 3–17.

Spreen, G., Kaleschke, L., & Heygster, G. (2008). Sea ice remote sensing using AMSR-E 89-GHz channels. *Journal of Geophysical Research*, *113*, C02S03. https://doi.org/10.1029/2005JC003384

Stroeve, J. C., Markus, T., Maslanik, J., Cavalieri, D., Gasiewski, A., Heinrichs, J., et al. (2006). Impact of surface roughness on AMSR-E sea ice products. *IEEE Transactions on Geoscience and Remote Sensing*, *44*(11), 3103–3117.

Sturm, M., Holmgren, J., & Perovich, D. (2002). Winter snow cover on the sea ice of the Arctic Ocean at the Surface Heat Budget of the Arctic Ocean (SHEBA): Temporal evolution and spatial variability. *Journal of Geophysical Research*, *107*(C10), 8047. https://doi.org/10.1029/2000JC000400

Tonboe, R. T., Heygster, G., Pedersen, L. T., & Andersen, S. (2006). Sea ice emission modelling. In Mätzler, C. (Ed.), *Thermal microwave radiation: Applications for remote sensing* (Vol. 52, pp. 382–425). London, UK: IEE Electromagnetic Waves Series.

Turner, D. D., Cadeddu, M. P., Lohnert, U., Crewell, S., & Vogelmann, A. M. (2009). Modifications to the water vapor continuum in the microwave suggested by ground-based 150-GHz observations. *IEEE Transactions on Geoscience and Remote Sensing*, *47*(10), 3326–3337.

Ulaby, F., & Long, D. G. (2014). *Microwave radar and radiometric remote sensing*. Annn Arbor, Michigan: University of Michigan Press.

Ulaby, F., & Long, D. G. (2014). *Microwave remote sensing. Active and passive* (Vol. 3). Annn Arbor, Michigan: University of Michigan Press.

Wang, D., Prigent, C., Kilic, L., Fox, S., Harlow, C., Jimenez, C., et al. (2017). Surface emissivity at microwaves to millimeter waves over polar regions: Parameterization and evaluation with aircraft experiments. *Journal of Atmospheric and Oceanic Technology*, *34*(5), 1039–1059.

Webster, M., Gerland, S., Holland, M., Hunke, E., Kwok, R., Lecomte, O., et al. (2018). Snow in the changing sea-ice systems. *Nature Climate Change*, *8*, 946–953.

Wever, N., Rossmann, L., Maaß, N., Leonard, K. C., Kaleschke, L., Nicolaus, M., & Lehning, M. (2019). Version 1 of a sea ice module for the physics based, detailed, multi-layer SNOWPACK model. *Geoscience Model Development Discussion*, *2019*, 1–30.

Wiesmann, A., & Mätzler, C (1999). Microwave emission model of layered snow packs. *Remote Sensing of Environment*, *123*(3), 307–316.

Wiesmann, A., Mätzler, C., & Weise, T. (1998). Radiometric and structural measurements of snow samples. *Radio Science*, *33*(2), 273–289.

Willmes, S., Nicolaus, M., & Haas, C. (2014). The microwave emissivity variability of snow covered first-year sea ice from late winter to early summer: A model study. *The Cryosphere*, *8*(3), 891–904.

Worby, A. P., Markus, T., Steer, A. D., Lytle, V. I., & Massom, R. A. (2008). Evaluation of the AMSR-E snow depth product over East Antarctic sea ice using in situ measurements and aerial photography. *Journal of Geophysical Research*, *11*, C05S94. https://doi.org/10.1029/2007JC004181